

Bifurcation Points of Periodic Triangular Patterns Obtained in Reaction-Diffusion System with Anisotropic Diffusion

Hiroto Shoji^{1*}, Shunya Yokogawa¹, Ryo Iwamoto¹, Kohtaro Yamada²

¹Department of Science and Technology, Kwansei Gakuin University, Hyogo, Japan

²Liberal Arts and Sciences, National Institute of Technology, Anan College, Tokushima, Japan

Email: *shoji@kwansei.ac.jp

How to cite this paper: Shoji, H., Yokogawa, S., Iwamoto, R. and Yamada, K. (2022) Bifurcation Points of Periodic Triangular Patterns Obtained in Reaction-Diffusion System with Anisotropic Diffusion. *Journal of Applied Mathematics and Physics*, 10, 2341-2355.

<https://doi.org/10.4236/jamp.2022.107159>

Received: June 23, 2022

Accepted: July 26, 2022

Published: July 29, 2022

Copyright © 2022 by author(s) and Scientific Research Publishing Inc.

This work is licensed under the Creative Commons Attribution-NonCommercial International License (CC BY-NC 4.0).

<http://creativecommons.org/licenses/by-nc/4.0/>



Open Access

Abstract

Turing demonstrated that spatially heterogeneous patterns can be self-organized, when the two substances interact locally and diffuse randomly. Turing systems have been applied not only to explain patterns observed within the biological and chemical fields, but also to develop image information processing tools. In a twin study, to evaluate the V-shaped bundle of the inner ear outer hair, we developed a method that utilizes a reaction-diffusion system with anisotropic diffusion that exhibited triangular patterns with the introduction of a certain anisotropy strength. In this study, we explored the parameter range over which these periodic triangular patterns were obtained. First, we defined an index for triangular clearness, TC . Triangular patterns can be obtained by introducing a large anisotropy δ , but the range of δ depends on the diffusion coefficient. We found an explanatory variable that can explain the change in TC based on a heuristic argument of the relative distance of the pitchfork bifurcation point between the maximum and minimum anisotropic diffusion function values. Clear periodic triangular patterns were obtained when the distance between the minimum anisotropic function value and pitchfork bifurcation point was over 2.5 times the distance to the anisotropic diffusion function maximum value. By changing the diffusion coefficients or the reaction terms, we further confirmed the accuracy of this condition using computer simulation. Its relevance to diffusion instability has also been discussed.

Keywords

Reaction-Diffusion, Turing, Periodic Triangular Pattern

1. Introduction

Turing showed that a coupled reaction-diffusion (RD) equation with two components admits spatially periodic solutions when certain conditions are satisfied [1]. Without diffusion, the local reaction of these two substances is stable and converges to an equilibrium. However, with diffusion, the uniform steady state becomes unstable. This mechanism is designated as a Turing system. Two dimensional (2D) RD models of the Turing system can generate stationary periodic patterns, such as stripe or spot patterns, and have been applied to generate biological textures, patterns and structures [2] [3].

In a twin paper, we proposed the use of the Turing system including anisotropic diffusion for the image analysis of V-shaped bundles [4]. The outer hair cells are arranged in three rows near the saccule [5]. We developed a method to quantify the arrangement of the V-shaped bundles of stereocilia utilizing information provided by the Turing model [4]. In the proposed RD system, periodic triangle patterns were obtained by selecting relevant parameters, which allowed us to evaluate the V-shaped bundle pattern.

In the present follow-up study, we further examined the anisotropic Turing model. In Shoji and Iwamoto [4], we primary used one set of the parameters to generate the periodic triangular patterns. However, the period of V-shaped bundles in the images acquired by each experimenter will be varied. For the effective extraction of a given image, adjusting the parameters is necessary to obtain patterns with a suitable frequency period. Parameters in the diffusion terms are useful for this purpose [2]. In contrast to studying using the parameters, we explored the conditions that allowed for the emergence of periodic triangular patterns.

The organization of the present paper is as follow. In Section 2, we described the reaction-diffusion model with anisotropic diffusion. In Section 3, the model was solved numerically. The behavior of pattern formation differs depending on the anisotropic strength. The linear stability analysis of the model revealed that the obtained modes were unchanged regardless of the anisotropic strength, which could be seen in first stage of pattern formation. Then, final patterns were compared by the frequency distributions considering the null clines of the reaction terms. We found the distribution near the equilibrium point of reaction term was different in the case where stable triangular pattern obtained. In order to characterize this feature based on the index of the obtained patterns, a statistical index of triangular clearness to quantify clear triangular pattern was prepared in Section 4. We derived an explanatory variable based on a heuristic argument regarding the relative position of pitchfork bifurcation in Section 5. In Section 6, we compared the prepared index and the explanatory variable. Using the statistical procedure, we derived the condition for emerging triangular patterns. In Section 7, we examined Schnackenberg model whether the same conclusion holds. Finally, the results are discussed in Section 8.

2. Model

2.1. Reaction-Diffusion System

Turing [1] showed that two diffusive chemicals that react locally can generate a spatially heterogeneous pattern in a uniform field. The system is written as follows:

$$u_t = d_u \nabla^2 u + f(u, v), \quad (1)$$

$$v_t = d_v \nabla^2 v + g(u, v), \quad (2)$$

where u and v are the concentrations of two substances that differ in diffusivity. In this case, we assume that v diffuses faster than u ; hence, d_v is larger than d_u .

We consider the solution (u_0, v_0) such that $f(u_0, v_0) = 0$ and $g(u_0, v_0) = 0$. We are concerned with the monostable situation when the diffusion are absent. Putting $(u - u_0, v - v_0) \sim \exp(i(k_x x + k_y y) + \lambda t)$, the linear stability analysis of the uniform solution is carried out. The eigenvalue λ is a solution of the algebraic equation

$$\lambda^2 + \{(d_u + d_v)k^2 - (f_u + g_v)\} \lambda + (d_u k^2 - f_u)(d_v k^2 - g_v) - f_v g_u = 0, \quad (3)$$

where $k = \sqrt{k_x^2 + k_y^2}$, $f_u = \partial f / \partial u|_{(u_0, v_0)}$, $f_v = \partial f / \partial v|_{(u_0, v_0)}$, $g_u = \partial g / \partial u|_{(u_0, v_0)}$ and $g_v = \partial g / \partial v|_{(u_0, v_0)}$. Solution (u_0, v_0) becomes unstable when the real part of λ is positive. The eigenvalue becomes positive at the critical wave number given by $k_c^2 = (d_v f_u + d_u g_v) / (2d_u d_v)$. The parameter region where (u_0, v_0) is linearly unstable is given by the condition

$$\frac{(d_v f_u + d_u g_v)^2}{4d_u d_v} - (f_u g_v - f_v g_u) > 0. \quad (4)$$

The model satisfying the condition above is referred to as the Turing system [2].

At the bifurcation point where the uniform solution (u_0, v_0) becomes unstable, we require the equality in Equation (4). For fixed parameters, except d_u , this defines a critical diffusion coefficient d_u^c , that is, the pitchfork bifurcation point [2]. The pitchfork bifurcation point d_u^c is derived as the appropriate root of

$$g_v^2 (d_u^c)^2 + 2(d_v f_u g_v - 2d_v f_u g_v + 2d_v f_v g_u) d_u^c + d_v^2 f_u^2 = 0 \quad (5)$$

2.2. Anisotropic Diffusion

In Shoji and Iwamoto [4], we introduced anisotropic diffusion based on the planar cell polarity of hair cells [5]. We considered a situation where the speed of the diffusion process changes depending on the direction of connection with the adjacent reaction cells.

Shoji and Iwamoto [4] showed that periodic triangular patterns can be obtained by setting sufficiently strong anisotropy. Here we further examined the

periodic triangular patterns obtained using an RD system with anisotropic diffusion considering the following dynamics:

$$u_t = d_u \nabla \cdot (D_u(\theta_u) \nabla u) + u(1 - u^2) - v, \quad (6)$$

$$v_t = d_v \nabla^2 v + \gamma(u - \alpha v - \beta). \quad (7)$$

The diffusion coefficient of u is

$$D_u(\theta_u) = (1 - \delta \cos 3\theta_u)^{-1/2} \quad (8)$$

where θ_u indicates the angle of the gradient vectors of u according to

$$\theta_u = \arctan\left(\frac{\partial u}{\partial y} / \frac{\partial u}{\partial x}\right). \quad (9)$$

The flux of u is proportional to the gradient vector, but the multiplication coefficient depends on the angle of the vector. Equation (9) implies that the diffusivity of u is the largest for $\theta_u = 0, 2\pi/3$, and $4\pi/3$ and that it is the smallest for the directions to $\theta_u = \pi/3, \pi$ and $5\pi/3$. δ is the magnitude of anisotropy for u . This satisfies the condition $0 \leq \delta < 1$. The special case of $\delta = 0$ implies an isotropy in the diffusion.

This form of anisotropic diffusion was adopted by Kobayashi [6] when studying dendritic crystal formation, but the functional forms of $D_u(\theta_u)$ that he adopted were different. Furthermore, in our previous study [7], this form of anisotropy was adopted to explain the directionality of stripes on fish skin.

In the following step, we first studied cases with the reaction terms proposed by FitzHugh-Nagumo [8], and written as

$$f(u, v) = u - u^3 - v, \text{ and } g(u, v) = \gamma(u - \alpha v - \beta), \quad (10)$$

where the constants α , β , and γ are all positive. This set of equations was initially introduced as a model equation for impulse propagation along nerve axon [8]. Subsequently, we discuss other choices of reaction terms.

3. Obtained Patterns

We numerically calculated the model given by Equations (6)-(10). We chose the following parameters: $\alpha = 0.50$, $\beta = 0.01$, and $\gamma = 26.0$, studied in Shoji and Iwamoto [4]. We examined the obtained patterns using different parameter values, d_u and d_v . All the simulations were performed with a periodic boundary condition in a square domain of size: 1.28×1.28 (grid size: 128×128). A simple explicit scheme was used. These parameters were chosen to satisfy the stability conditions for the numerical analysis. The initial distributions of u and v were given as the equilibrium (u_0, v_0) with small random deviations, except in Section 6.3.

We performed a numerical simulation for $t = 1000$, considered a sufficiently long time to reach the final patterns. **Figure 1** shows the time evolution of the patterns in a density plot of u . The distributions of v followed the same periodic patterns with the same periodicities, but different amplitudes. Without anisotropy,

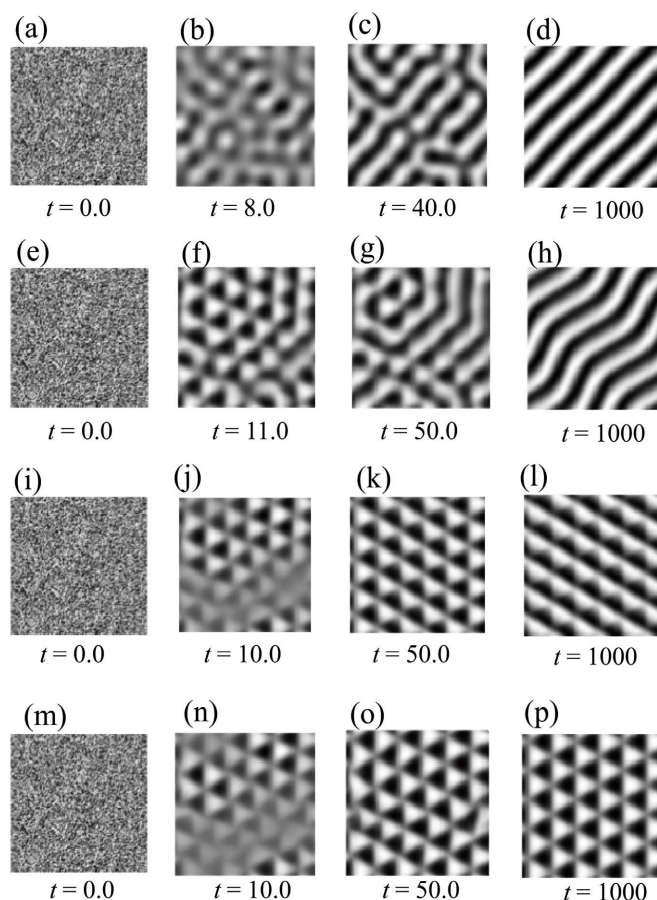


Figure 1. Time evolution of $u(r,t)$. (a)-(d) were obtained numerically from Equations (6)-(10) with $\delta = 0.00$; (e)-(h) were obtained with $\delta = 0.50$; (i)-(l) were obtained with $\delta = 0.75$; and (m)-(p) were obtained with $\delta = 0.90$. Without anisotropy, a stripe pattern was obtained, as shown in (a)-(d). In the case of $\delta = 0.50$, a stripe pattern emerged from an initially periodic triangular pattern, as shown in (e)-(h). In the case of $\delta = 0.75$, broken triangles form an initially periodic triangles pattern, as shown in (i)-(l). In the case of $\delta = 0.90$, a periodic triangular pattern emerges, as shown in (m)-(p).

the stripe patterns that we obtained are shown in **Figure 1(d)**. When anisotropy was introduced, the generated modes initially formed periodic triangular patterns, as shown in **Figure 1(f)**, **Figure 1(j)**, and **Figure 1(n)**. When the strength of anisotropy was not sufficiently large, the triangular patterns were disturbed and finally formed a stripe pattern similar to the native pattern without anisotropy, as shown in **Figures 1(f)-(h)**, or broken triangles, as shown in **Figures 1(j)-(l)**. However, when the anisotropy strength was sufficiently large, the periodic triangular patterns were sustained asymptotically, as shown in **Figures 1(n)-(p)**.

3.1. Unstable Modes Obtained by Linear Analysis

The Turing patterns are known to be related to the critical wavelength at the early

stage of pattern formation [2]. We explored the critical modes of (k_x, k_y) attaining a constant term of Equation (3) of the lowest magnitude. By setting $(u - u_0, v - v_0) \sim \exp(i(k_x + k_y)x + \lambda t)$, we numerically explored (k_x, k_y) with the lowest values of the constant term

$$\left(\frac{d_u(k_x^2 + k_y^2)}{\sqrt{1 - \delta \cos\left(3 \tan^{-1}\left(\frac{k_y}{k_x}\right)\right)}} - f_u \right) \left\{ d_v(k_x^2 + k_y^2) - g_v \right\} - f_v g_u. \quad (11)$$

Figure 2 shows the contour plot of the values of constant term of Equation (11) respect to k_x and k_y . In the case where $\delta = 0.00$, the point with low values of Equation (11) are located in concentric circles equidistant from the (0,0), as shown in **Figure 2(a)**. Therefore, no directionality can be observed in the obtained pattern shown in **Figure 1(b)** and **Figure 1(c)**. However, when $\delta = 0.50$ and $\delta = 0.90$, the point with low values of Equation (11) are located at the four points (two modes) from the (0,0), as shown in **Figure 2(b)** and **Figure 2(c)**. Numerically, we explore the points with the lowest values of Equation (11). Then the lowest values -41.3 takes at the $(k_x, k_y) = \{(39.5, 68.4), (-39.5, 68.4), (-39.5, -68.4), (39.5, -68.4)\}$, which is correspond to $\theta_u = \tan^{-1}(k_y/k_x) = 2\pi/3, 4\pi/3$. This analysis revealed that the obtained mode were unchanged regardless of the anisotropy strength.

As shown in **Figure 1(f)**, **Figure 1(j)** and **Figure 1(n)**, the exponential growth of the specific unstable critical mode revealed by the linear analysis emerged from the random initial states when anisotropy was introduced in the early stages of pattern formation. However, as shown in **Figures 1(f)-(h)** or **Figures 1(j)-(l)**, the triangular patterns were eventually disturbed or changed, resulting in a stripe pattern or a mixed pattern of stripes and triangles. This process appears to be related to the nonlinear evolution of domains that occurs in the second stage, converging to asymptotic patterns [2] [9]. Indeed, the linear analysis failed to determine whether a triangular pattern could be obtained or not.

3.2. Frequency Distributions of Patterns

Shoji *et al.* [10] compared the nullclines of the reaction terms and asymptotic

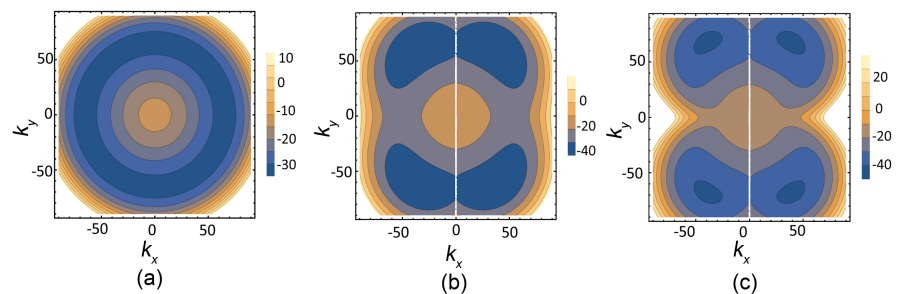


Figure 2. Contour plots of Equation (11) with respect to k_x and k_y . (a) $\delta = 0.00$, (b) $\delta = 0.50$, and (c) $\delta = 0.90$.

distributions. We used the frequency distribution of u sampled from a number of points in the domain to obtain the patterns and quantify the differences in the frequency distributions among the obtained patterns. We applied this concept to further explore the conditions that allow triangular patterns to be obtained.

Figure 3(a) and **Figure 3(b)** show the isoclines of the reaction terms of Equations (6), (7) and (10) (in dotted lines) and the distribution plots of (u, v) in the (u, v) -plane, obtained from the numerical calculations of Equations (6)-(10). **Figure 3(c)** and **Figure 3(d)** show the distributions of u sampled from a number of points in the domain obtained from the numerical calculations of Equations (6)-(10).

The isocline shows a sharp increase when u is larger than around -0.5 and a sharp decline when u was smaller than 0.5 . In the case of the Turing diffusion-induced instability, that is, the intersection of $f(u, v)$ and $g(u, v)$, the distribution is maintained within this range though diffusion [2]. Patterns obtained by the RD system without anisotropy were M-shaped, as shown in **Figure 3(c)**, with two peaks at the highest and lowest values [10]. By contrast, the patterns obtained by the RD system with anisotropy ($\delta = 0.90$) exhibited three peaks: which were the peak around u_0 , including the two peaks explained above. Therefore, we could presume that the triangle pattern had not only the Turing pattern properties, but also equilibrium distribution properties.

4. Method of Imaging Process

Here, we introduce the statistics used to characterize the spatial patterns obtained

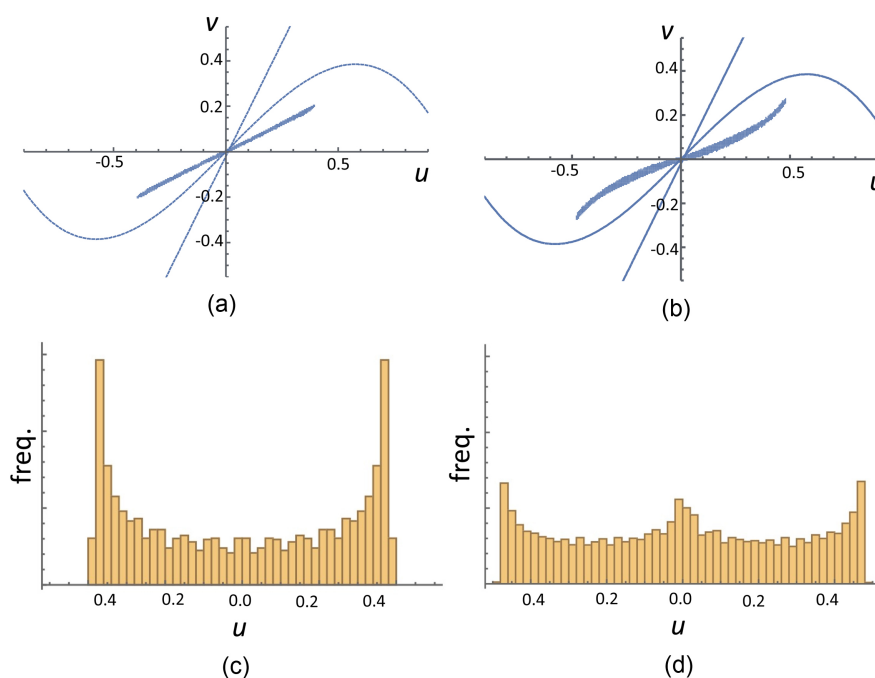


Figure 3. Isoclines with points of distribution values (a)-(b) and frequency distributions (c)-(d). (a) and (c) were obtained from Equations (6)-(10) without anisotropy ($\delta = 0.00$), (b) and (d) were obtained from Equations (6)-(10) with anisotropy ($\delta = 0.90$).

by the model to distinguish triangular patterns from the obtained patterns. We performed a Fourier transformation of the value of u to examine the structure of the obtained patterns. For example, in simple case of a stripe pattern, that is, $u(\mathbf{r}) = A \cos(\mathbf{q} \cdot \mathbf{r})$ indicating the amplitude A and wave vector \bar{q} , the Fourier transform is as follows:

$$\hat{u}(\mathbf{q}) = \int d\mathbf{r} u(\mathbf{r}) \exp(i\mathbf{q} \cdot \mathbf{r}). \quad (12)$$

Displaying the intensity $|\hat{u}(\mathbf{q})|$ in the wavenumber space, the properties of the obtained patterns were examined. As shown above, a typical stripe pattern obtained exhibits a strong first peak.

We performed a Fourier analysis of the triangular pattern shown in **Figure 4(a)** by comparing another typical Turing pattern, the spot pattern shown in **Figure 4(b)**, which was obtained by Equations (6)-(10) using the same parameters as the obtained stripes ($\delta = 0.00$), except for $\beta = 0.08$. **Figure 4(c)** shows the intensity of the Bragg peak for $q = |\mathbf{q}|$. The blue line and red line in **Figure 4(c)** show the case of the spot and triangular patterns, respectively. It is found that peaks is appeared for similar value of q in both cases. However, the intensities of the higher peaks ($q > 1$) of the triangular pattern (red line) are larger than those of the spot pattern (blue line), although the first peak ($q \approx 0.6$) of triangular pattern is nearly the same as that of the spot pattern. Therefore, to determine whether periodic triangular patterns were obtained, we introduce the triangular clearness $TC = (p_2^2 + p_3^2) / p_1^2$, where p_1 , p_2 , and p_3 represent the intensity of the first peak ($q \approx 0.6$ in the case of **Figure 4(c)**), and the second peak ($q \approx 1.05$ in the case of **Figure 4(c)**), and the third peak ($q \approx 1.25$) in the case of **Figure 4(c)**), respectively. Therefore, when TC is larger, we regarded the pattern as composed of a clear triangular. When TC was small, we regarded the pattern as stripe patterns, or the patterns exhibited broken triangles and become stripes.

Comparing TC values with the obtained patterns shown in **Figure 1**, TC was lower for stripe patterns such as those in **Figure 1(d)** ($TC = 4.24 \times 10^{-15}$) and (h)

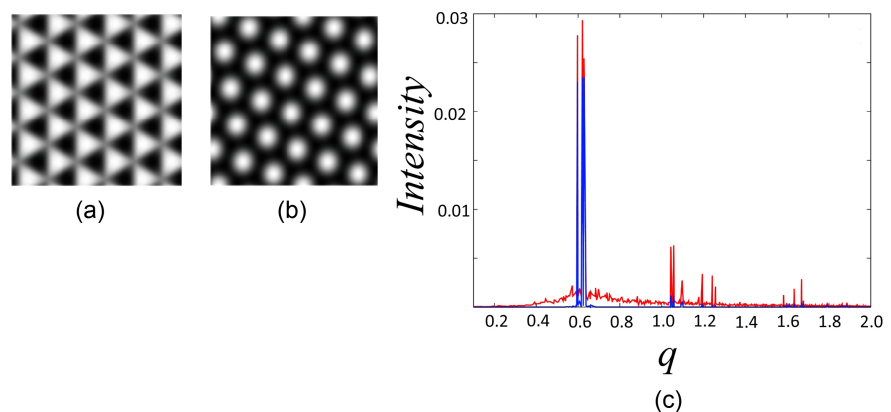


Figure 4. (a) The triangular pattern obtained by the numerical simulation; (b) The spot pattern obtained by the numerical simulation; (c) The intensity of Bragg spots. The blue line and the red line show the case of the spot pattern and the triangular pattern, respectively.

($TC = 7.03 \times 10^{-4}$). On the other hand, the TC value increases when the triangles were partially visible, as in **Figure 1(i)** ($TC = 1.26 \times 10^{-2}$), and if the pattern consists of clear triangles, as in **Figure 1(p)** ($TC = 3.05 \times 10^{-2}$), the TC value became large.

5. A Heuristic Argument regarding When Stable Triangular Patterns Obtained

We developed a heuristic argument to determine the range of the obtained periodic triangular patterns. We introduced the anisotropic diffusion coefficient function, Equation (8), in the proposed RD model, in which the values of the diffusion coefficient function $D_u(\theta_u)$ is between the maximum

$$D_u^{\max} = d_u / \sqrt{1 - \delta} \quad \text{and the minimum} \quad D_u^{\min} = d_u / \sqrt{1 + \delta}.$$

We considered the parameter set used in the computer simulation in **Figure 1**, where $d_u = 5.00 \times 10^{-4}$, $d_v = 5.00 \times 10^{-2}$, and pitchfork bifurcation $d_u^c = 6.60 \times 10^{-4}$ obtained using Equation (5). **Figure 5** shows the relative ranges of the values of coefficient function (8). In the case of $\delta = 0.00$ (no anisotropy), the parameters chosen resulted in Turing instability, and the diffusion coefficient function, Equation (8), is always constant, as indicated by a single point in **Figure 5**. In the case of $\delta = 0.50$, D_u^{\max} and D_u^{\min} were 7.07×10^{-4} and 4.08×10^{-4} , in the case of $\delta = 0.75$, D_u^{\max} and D_u^{\min} were 1.00×10^{-3} and 3.78×10^{-4} , and in the case of $\delta = 0.90$, D_u^{\max} and D_u^{\min} were 1.58×10^{-3} and 3.62×10^{-4} , respectively. It is noted that when d_v was fixed Turing instability occurs when d_u was decreasing. The ranges were located within the region where the equilibrium was stable and the region where Turing instability occurs beyond the pitchfork bifurcation, d_u^c , as given by Equation (5). To quantify the ratio of the distances between D_u^{\max} and d_u^c and between d_u^c and D_u^{\min} , we define the following index

$$A = (d_u^c - D_u^{\min}) / (D_u^{\max} - d_u^c) \tag{13}$$

We note that A satisfies $A \geq -1$. In the case of $\delta = 0.00$ (no anisotropy), A is -1.0 , whereas A increases as the anisotropy δ increased. In the case of $\delta = 0.50$,

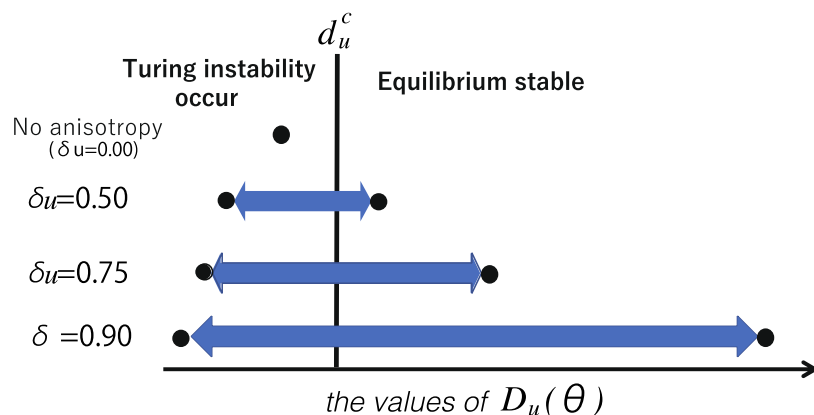


Figure 5. Schematic showing the ranges of Equation (8).

$d_u = 5.00 \times 10^{-4}$, and $d_v = 5.00 \times 10^{-2}$, a triangular pattern first appeared before being disturbed and was replaced by a stripe pattern as shown in **Figures 1(e)-(h)** for $A = 0.197$. In the case of $\delta = 0.75$, a triangular pattern replaced a broken triangles, as shown in **Figures 1(i)-(l)** for $A = 1.22$. In the case of $\delta = 0.90$, a triangular pattern was sustained, as shown in **Figures 1(m)-(p)** for $A = 3.13$.

6. Results

6.1. Triangular Clearness Index TC

For the patterns obtained by the RD model given by Equations (6)-(10), we calculated the triangular clearness TC as explained in Section 4. **Figures 6(a)-(c)** show how TC changes as δ changes for the three different cases of diffusion coefficients. The results were obtained when d_u was changed to 6.00×10^{-4} in **Figure 6(b)** and d_v to 7.50×10^{-2} in **Figure 6(c)**, based on the diffusion coefficients $d_u = 5.00 \times 10^{-4}$ and $d_v = 5.00 \times 10^{-2}$ in **Figure 6(a)**.

It could be seen that, at small δ , TC was low, whereas, at sufficiently large δ , TC had high values in the three examined cases. However, the points and rates of change from low TC values to high TC values were distinctively different.

Next, we examined the changes in TC using A , as described in Section 5. **Figures 6(d)-(f)** show the results for the same diffusion coefficients as those in **Figures 6(a)-(c)**, respectively. The changes in the value of TC displayed an S-shaped function, whereas the TC value changed from low to high around $A = 0.0 - 3.0$ in all the cases.

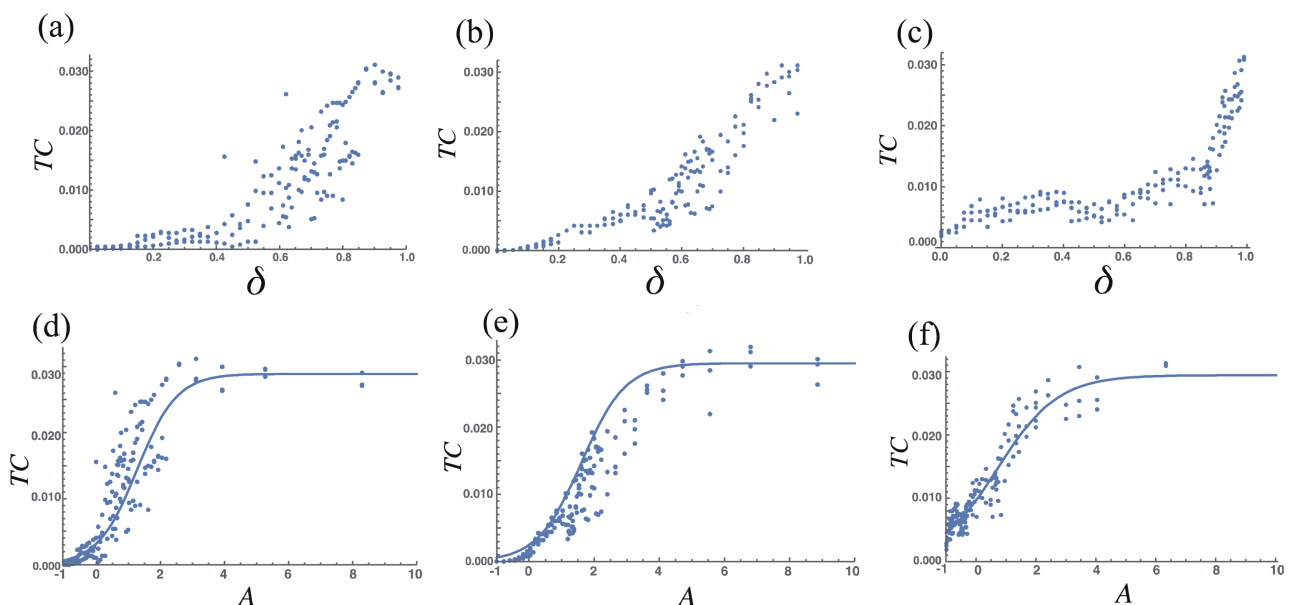


Figure 6. Triangular clearness: TC as defined in Section 4 versus the anisotropy δ in the FitzHugh-Nagumode model (a)-(c) and the index A in Equation (13) (d)-(f). The parameters were as follows: $\alpha = 0.50$, $\beta = 0.01$, and $\gamma = 26.0$, which were also used in reference [4], as well as (a) and (d) $d_u = 5.00 \times 10^{-4}$, $d_v = 5.00 \times 10^{-2}$, (b) and (e) $d_u = 6.00 \times 10^{-4}$, $d_v = 5.00 \times 10^{-2}$, and (c) and (f) $d_u = 5.00 \times 10^{-4}$, $d_v = 7.50 \times 10^{-2}$.

6.2. Regression Analysis

A nonlinear regression was performed using the follows equation:

$$TC \sim a/(1+be^{rA}), \quad (14)$$

where a , b and r are parameters. To fit the obtained data in Equation (14), we utilized the software “R” in MacOSX.

In **Figures 6(d)-(f)**, the regression function is represented by a solid lines. The fitted parameters are listed in **Table 1**. All parameters listed in **Table 1** appear to be significantly different ($p < 0.001$).

Let $Q_0(A_0, TC_0)$ be the coordinates of the inflection point of the function (14). Then, A_0 and TC_0 could be obtained as $A_0 = \ln b/r$, and $TC_0 = a/2$, respectively [11] [12]. The function (14) is symmetric with respect to its inflection point and reaches 50% of its maximal value a . Moreover, the inflection point coordinates of the derivative function of Equation (14), $Q_1(A_1, TC_1)$, and $Q_2(A_2, TC_2)$ also calculated [12]. A_1, A_2 is

$$A_1 = A_0 - 1.318/r, \text{ and } A_2 = A_0 + 1.318/r, \quad (15)$$

whereas the TC values at these points could be calculated as follows:

$$\begin{aligned} TC_1 &= a(1 - \sqrt{1/3})/2 \sim 0.211a, \\ TC_2 &= a(1 + \sqrt{1/3})/2 \sim 0.789a. \end{aligned} \quad (16)$$

Therefore, these points were subject to change until they reached approximately 21% and 79% of the final TC values in Q_1 and Q_2 , respectively [12]. The coordinates of Q_0 and Q_2 are listed in **Table 1**. We found that the parameters for a and Q_2 were similar for the three cases shown in **Figures 6(d)-(f)**, although Q_0 , and the parameters in Equation (14) were different.

6.3. Triangular Patterns Given as Initial Distributions

In the previous section, the initial distributions were set as the equilibrium point with small perturbations using three different seed types. Here, we provided the initial distributions of u and v for the triangular patterns.

We started the numerical simulations for Equations (6)-(10) by introducing a

Table 1. A summary of the parameters fitted to the function of Equation (14) for the obtained patterns in the FitzHugh-Nagumo model, Equations (6)-(10).

Figure	a	b	r	Q_0	Q_2
Figure 6(d)	2.89×10^{-2}	7.92	-1.45	(1.25, 1.45×10^{-2})	(2.34, 2.28×10^{-2})
Figure 6(e)	2.95×10^{-2}	11.01	-1.48	(1.61, 1.48×10^{-2})	(2.49, 2.23×10^{-2})
Figure 6(f)	2.81×10^{-2}	2.05	-0.93	(0.72, 1.47×10^{-2})	(2.19, 2.32×10^{-2})
Figure 7(a)	3.58×10^{-2}	4.28	-1.30	(1.11, 1.79×10^{-2})	(2.12, 2.82×10^{-2})
Figure 7(b)	3.64×10^{-2}	4.56	-1.32	(1.07, 1.82×10^{-2})	(2.16, 2.99×10^{-2})
Figure 7(c)	3.59×10^{-2}	6.01	-1.51	(1.19, 1.79×10^{-2})	(2.06, 2.83×10^{-2})

Gaussian noise source ξ_u in Equation (6) and ξ_v in Equation (7) of the three types of amplitudes of random forces up to 4×10^5 time steps. We then turned off the random forces and continued the numerical simulations up to the same steps as the above and observed the index TC . We tested three sets of random force strengths: $\xi_u = \xi_v = 1.00 \times 10^{-2}$, 2.00×10^{-2} , and 3.00×10^{-3} . The relationship between each TC and A is shown in **Figures 7(a)-(c)**.

In the case of $\xi_u = \xi_v = 1.00 \times 10^{-2}$ and 2.00×10^{-2} , it can be seen that the TC value varies in curves, except for $A = 0.80 - 1.60$. However, for $\xi_u = \xi_v = 3.00 \times 10^{-2}$, the change in TC also shows a combination of subtle changes in the values, similar to the changes shown in **Figures 6(d)-(f)**, where the initial distribution were set as equilibria with small perturbations. This suggests that the effect of the initial distribution can be seen as shown in **Figure 7(a)** and **Figure 7(b)**. However, in **Figure 7(c)**, the random force is too strong and the effect of the initial distribution is lost.

A nonlinear regression was also performed as explained above. The values of a , b , r and coordinates Q_0 and Q_2 are shown in **Table 1**. Even in these cases, it can be found that the parameter for a and Q_2 were similar.

6.4. Ranges of δ

In the previous section, we found that the last phase of changing the TC values in the logistic function was similar for all cases of diffusion coefficients. Therefore, we determined that A_2 is the bifurcation point for obtaining triangular patterns, and the maximum value of A_2 (2.5) as the threshold for A as the explanatory variable.

We then returned to the function of the value of δ according to Equation (13) and predicted the bifurcation point as a function of δ .

$$d_u / \sqrt{1 - \delta} - d_u^c \leq A_2 (d_u^c - d_u / \sqrt{1 + \delta}). \tag{17}$$

Transforming to the δ condition, we obtained:

$$\delta \geq 1 - 1/B^2 \tag{18}$$

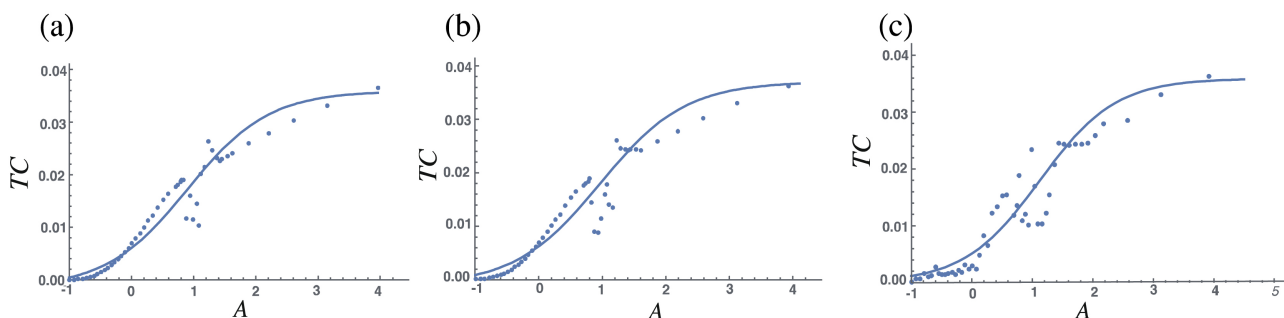


Figure 7. Triangular clearness: TC as defined in Section 4 versus the index A in Equation (13) when the initial distribution of triangular patterns were given and different strengths of random forces added to Equations (6)-(10) before the numerical simulation were performed. The parameters were as follows: $\alpha = 0.50$, $\beta = 0.01$, and $\gamma = 26.0$, as well as (a) $d_u = 5.00 \times 10^{-4}$, $d_v = 5.00 \times 10^{-2}$, (b) $d_u = 6.00 \times 10^{-4}$, $d_v = 5.00 \times 10^{-2}$, and (c) $d_u = 5.00 \times 10^{-4}$, $d_v = 7.50 \times 10^{-2}$.

where $B = (A_2 + 1)d_u^c/d_u - A_2/\sqrt{2}$. Once d_u and d_v were determined, d_u^c could be calculated using Equation (5). Subsequently, the bifurcation point of δ was determined.

In the case of $\alpha = 0.50$, $\beta = 0.01$, $\gamma = 26.0$, $d_v = 5.00 \times 10^{-2}$, and $d_u = 5.00 \times 10^{-4}$ which are the same parameters in Figure 6(d) and Figure 7, as well as those used in [4], the bifurcation point of δ was 0.856.

7. Another Model of Turing Type

Thus far, we have concentrated on the FitzHugh-Nagumo equation given by Equation (10). The result suggests that the index A can predict the range of the triangular pattern obtained in the Equations (6)-(10). In this section, we examine whether the same conclusion holds for another choice of reaction terms, we examined the following alternative model, which is known as “the substrate-depleted model” [13] given by the following reaction terms

$$f(u, v) = \alpha - u + u^2v, \text{ and } g(u, v) = \beta - u^2v, \quad (19)$$

where α , and β were positive constants. The parameters in the reaction terms were set as $\alpha = 2.5 \times 10^{-2}$, and $\beta = 1.55$ were set to obtain stripe patterns without anisotropy ($\delta = 0.00$) [2] [10]. Here, we set the diffusion coefficients as follows: 1) $d_u = 7.00 \times 10^{-4}$, $d_v = 1.45 \times 10^{-2}$ (pitchfork bifurcation point of $d_u^c = 9.49 \times 10^{-4}$), 2) $d_u = 6.70 \times 10^{-4}$, $d_v = 1.45 \times 10^{-2}$ (pitchfork bifurcation point of $d_u^c = 9.49 \times 10^{-4}$), and 3) $d_u = 7.00 \times 10^{-4}$, $d_v = 1.40 \times 10^{-2}$ (pitchfork bifurcation point of $d_u^c = 9.16 \times 10^{-4}$).

Figure 8 shows the results of the changes in TC using A in Equation (13). The change in TC value displays an S-shaped function. A regression analysis was performed using the method described above. The regression function is shown as a solid line in Figures 8(a)-(c). The fitted parameters and the coordinates Q_0 and Q_2 are listed in Table 2. The fitted parameters Q_2 were similar in all cases.

Comparing the results between the models, the value of A_2 was similar as the parameter obtained by FitzHugh-Nagumo model. By using the argument described in the previous section, we estimated the range of δ over which triangular

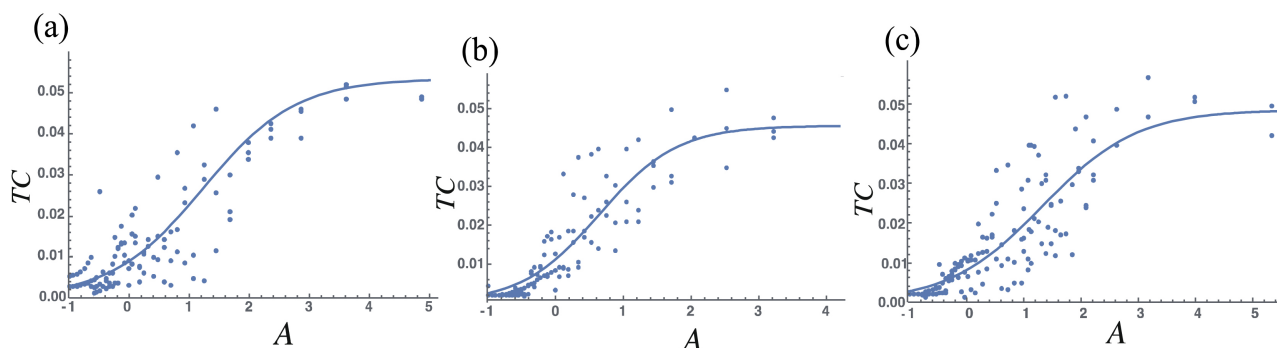


Figure 8. Triangular clearness: TC as defined in Section 4 versus the index A in Equation (13) in Schnackenberg model given by Equations (6)-(9) and (19) with $\alpha = 0.025$, $\beta = 1.55$, as well as (a) $d_u = 7.00 \times 10^{-4}$, $d_v = 1.45 \times 10^{-2}$, (b) $d_u = 6.7 \times 10^{-4}$, $d_v = 1.45 \times 10^{-2}$, and (c) $d_u = 7.00 \times 10^{-4}$, $d_v = 1.40 \times 10^{-2}$.

Table 2. A summary of the parameters fitted to the function of Equation (14) for the obtained patterns in the Schnackenberg model, Equation (6)-(9) with reaction terms (19).

Figure	a	b	r	Q_0	Q_2
Figure 8(a)	5.34×10^{-2}	4.94	-1.18	(1.34, 2.67×10^{-2})	(2.47) , 4.22×10^{-2}
Figure 8(b)	4.56×10^{-2}	3.38	-1.13	(1.07, 2.28×10^{-2})	(2.23) , 3.60×10^{-2}
Figure 8(c)	4.85×10^{-2}	5.03	-1.31	(1.33, 2.42×10^{-2})	(2.41) , 3.83×10^{-2}

patterns were obtained as $\delta \geq 0.883$ when $d_u = 7.00 \times 10^{-4}$ and $d_v = 1.45 \times 10^{-2}$, $\delta \geq 0.889$ when $d_u = 6.70 \times 10^{-4}$ and $d_v = 1.45 \times 10^{-2}$, and $\delta \geq 0.868$ when $d_u = 7.00 \times 10^{-4}$ and $d_v = 1.40 \times 10^{-2}$.

8. Discussion

The parameter region where the triangular patterns were obtained was investigated. By examining the asymptotic patterns, we inferred that the distributions of the obtained patterns were related to the ratio of the width belonging to the equilibrium of the diffusion coefficient to the width belonging to the diffusion-induced instability, A . Even if the diffusion coefficients changed and other reaction terms were used, clear triangular patterns were obtained when A value was large.

In this study, the threshold value of A was set to 2.5 which satisfies approximately 80% of the fitting parameter and statically equal to the maximum value of TC and the parameters examined in this study. Although this threshold was determined using the aforementioned statistical process, **Figures 6-8** show that when $A = 2.5$ or higher, the value of TC is consistently high.

Considering the time evolution of the morphogenesis of triangular patterns, as described in Section 3, nonlinear analysis is required for rigid mathematical analysis. In the present study, we focused on different aspects, namely the clearness of the triangular pattern that filled the entire space of parameters. In the present study, we discovered that a very simple index A could be useful for predicting the parameter region where the triangular patterns were obtained, and the condition of anisotropic strength δ for obtaining triangular patterns could be easily derived from the relation A in a straightforward manner, as shown in Equation (18).

In this study, anisotropy was introduced only for the diffusion of u , which has a small diffusion coefficient. However, it is also possible to introduce anisotropy only in the diffusion of v with a large diffusion coefficient, or in the diffusion of both u and v . The effect of the diffusion coefficient introduced here may become clearer in future studies.

This study indicates that defining a simple index characterizing the spatial patterns formed and relating this index to the properties of the model used would be useful for gaining a better understanding of pattern formation. This knowledge may be applied not only to biological pattern formation, but can also serve the development of methods for image information processing.

Acknowledgements

We thank Prof. M. Mimura and Prof. K. Osaki for helpful comments.

Conflicts of Interest

The authors declare no conflicts of interest regarding the publication of this paper.

References

- [1] Turing, A.M. (1952) The Chemical Basis of Morphogenesis. *Philosophical Transactions of the Royal Society of London*, **237**, 37-72. <https://doi.org/10.1098/rstb.1952.0012>
- [2] Murray, J. D. (2003) *Mathematical Biology*. Springer. <https://doi.org/10.1007/b98869>
- [3] Kondo, S. and Miura, T. (2010) Reaction-Diffusion Model as a Framework for Understanding Biological Pattern Formation. *Science*, **329**, 1616-1620. <https://doi.org/10.1126/science.1179047>
- [4] Shoji, H. and Iwamoto, R. (2022) Reaction-Diffusion Algorithm for Quantitative Analysis of Periodic V-Shaped Bundles of Hair Cells in the Inner Ear. *Journal of Biosciences and Medicines*, **10**, 240-251. <https://doi.org/10.4236/jbm.2022.103022>
- [5] Ross, M. and Pawlina, W. (2018) *Histology, A Text and Atlas with Correlated Cell and Molecular Biology*. 8th Edition, Wolters Kluwer.
- [6] Kobayashi, R. (1993) Modeling and Numerical Simulations of Dendritic Crystal Growth. *Physica D*, **63**, 410-423. [https://doi.org/10.1016/0167-2789\(93\)90120-P](https://doi.org/10.1016/0167-2789(93)90120-P)
- [7] Shoji, H., Iwasa, Y., Mochizuki, A. and Kondo, S. (2002) Directionality of Stripes Formed by Anisotropic Reaction-Diffusion Models. *Journal of Theoretical Biology*, **214**, 549-561. <https://doi.org/10.1006/jtbi.2001.2480>
- [8] Nagumo, J., Arimoto, S. and Yoshizawa, S. (1962) An Active Pulse Transmission Line Simulating Nerve Axon. *Proceedings of the IRE*, **50**, 2061-2070. <https://doi.org/10.1109/JRPROC.1962.288235>
- [9] Shoji, H., Yamada, K., Ueyama, D. and Ohta, T. (2007) Turing Patterns in Three Dimensions. *Physical Review E*, **75**, Article ID: 046212. <https://doi.org/10.1103/PhysRevE.75.046212>
- [10] Shoji, H., Iwasa, Y. and Kondo, S. (2003) Stripes, Spots, or Reversed Spots in Two-Dimensional Turing System. *Journal of Theoretical Biology*, **224**, 339-350. [https://doi.org/10.1016/S0022-5193\(03\)00170-X](https://doi.org/10.1016/S0022-5193(03)00170-X)
- [11] Crawley, M.J. (2007) *The R Book*. John Wiley & Sons, Ltd.
- [12] Gregorczyk, A. (1991) The Logistic Function—Its Application to the Description and Prognosis of Plant Growth. *Acta Societatis Botanicorum Poloniae*, **60**, 67-76. <https://doi.org/10.5586/asbp.1991.004>
- [13] Schnackenberg, J. (1979) Simple Chemical Reaction Systems with Limit Cycle Behavior. *Journal of Theoretical Biology*, **81**, 389-400. [https://doi.org/10.1016/0022-5193\(79\)90042-0](https://doi.org/10.1016/0022-5193(79)90042-0)